International Journal of Biology and Life Sciences
ISSN: 2957-9511 | Vol. 14, No. 2, 2026

Systematic Comparison of Chemical Constituents and Pharmacological Efficacy Among Different Parts of *Rosa odorata var. gigantea*: Stems as a Sustainable Medicinal Alternative to Roots

Jingmei Chen [1, 2, a, #], Yuhang Chen [1, 2, b, #], Xiaole Zhao [1, 2, c, #], Zhilin Bai [1, 2, d], Wenqian Wang [1, 2, e], Lianfan Wang [1, 2, f], Jingze Zhang [1, 2, g], Dailin Liu [1, 2, *]

[1] National Key Laboratory of Modern Chinese Medicine Innovation and Manufacturing, Tianjin University of Traditional Chinese Medicine, Tianjin 301617, China
[2] Tianjin Modern Innovation Chinese Medicine Technology Co., Ltd., Tianjin 300380, China

*** Corresponding author:** Dailin Liu (Email: dailinlch@163.com), [a] birerc@163.com, [b] 15154788751@163.com, [c] 17793644104@163.com, [d] 15234381508@163.com, [e] wwq20011016@163.com, [f] 1648795654@qq.com, [g] zhangjingze1977@163.com

[#] These authors contributed equally and should be considered co-first-authors.

Abstract: Gugongguo (GGG) (*Rosa odorata* Sweet var. *gigantea* (Coll. et Hemsl.) Rehd. et Wils.) is a perennial evergreen climbing shrub of Rosaceae. Its roots have long been utilized in Yi ethnic traditional medicine to treat gastrointestinal disorders like dysentery and diarrhea with remarkable efficacy. However, roots account for a small proportion of the whole plant, and root harvesting causes massive waste of stem and branch resources. To explore stems as potential alternative medicinal parts, this study analyzed the chemical components of GGG roots, stems and fruits via UPLC-Q-TOF-MS combined with GNPS molecular networking, determined total triterpenes and tannins contents by ultraviolet spectrophotometry, evaluated antidiarrheal activities using a castor oil-induced mouse model, and identified core bioactive components via Spearman correlation analysis. Results showed high chemical similarity between roots and stems (28 common components, complete triterpenoid overlap), with no significant differences in total triterpenes and tannins contents. Their small intestinal propulsion rates were comparable and significantly superior to that of fruits. Triterpenoids and tannins were identified as key bioactive components, with a high degree of overlap between roots and stems. This study confirms GGG stems as potential alternatives to roots, providing a scientific basis for improving resource utilization and promoting sustainable development of traditional medicinal resources.

Keywords: *Rosa odorata* Sweet var. *gigantea* (Coll. et Hemsl.) Rehd. et Wils.; UPLC-Q-TOF-MS; Chemical Components; Structural Identification; The Genus Rosaceae; Mass Spectrometry Fragmentation Pathways.

1. Introduction

Rosa odorata Sweet var. *gigantea* (Coll. et Hemsl.) Rehd. et Wils. is a perennial evergreen climbing shrub belonging to the genus *Rosa* of the family Rosaceae, commonly known as “Gugongguo” (GGG) in Yi ethnomedicine, predominantly distributed in Yunnan Province, China (e.g., Kunming, Dali, and Lijiang) [1]. GGG is medicinally utilized for its roots, which have long been employed in traditional Yi ethnomedicine to treat diarrhea, dysentery, and gastrointestinal disorders, attributed to their astringent, anti-inflammatory, and antidiarrheal properties. With the advancement of modern pharmacological research, the therapeutic potential of GGG roots has been fully validated—they not only eradicate pathogenic bacteria and protect the gastrointestinal mucosa but also accelerate mucosal healing. This efficacy has enabled their clinical application in commercial pharmaceutical preparations such as "Changshu Tablets" and "Changshu Capsules,". Yang[2] further establishing the core medicinal value of the roots.

Notably, the genus Rosa—to which GGG belongs—is renowned for its diverse array of bioactive constituents, including triterpenoids[3], tannins[4], and flavonoids. These components collectively endow plants of this genus with antioxidant, anti-inflammatory[5], and immunomodulatory activities [6]—a genus-level trait that aligns well with GGG’s therapeutic effects on digestive diseases. Specifically, triterpenoids (e.g., oleanolic acid derivatives) and hydrolyzable tannins have been identified as the dominant compounds in GGG roots, serving as the key material basis for its gastrointestinal protective effects [7]. Beyond the roots, the ripe fruits of GGG also hold significant development value: they are rich in nutrients such as minerals, amino acids, and proteins, and possess dual medicinal-edible potential. Currently, they are widely processed into functional foods (e.g., fruit wines), forming a resource utilization pattern of "roots for medicinal use and fruits for dietary use"[6].

However, as a perennial shrub, the roots of GGG account for a relatively small proportion of the entire plant, and harvesting the roots inevitably results in substantial waste of aboveground resources such as stems and branches. Currently, there is a lack of systematic research addressing whether these stem and branch resources possess medicinal value or can serve as potential alternative medicinal parts to the roots. Based on this, the present study aims to evaluate the feasibility of GGG aerial part as an alternative medicinal part to the roots through systematic experiments, thereby providing a scientific basis for balancing resource conservation and clinical needs, as well as improving the utilization efficiency of the whole-plant resources.

To investigate whether the stems of GGG can act as a potential medicinal part, this study provides the first systematic characterization of GGG stems, uncovering their previously unrecognized therapeutic potential. UPLC-Q-TOF-MS combined with GNPS molecular networking was used to systematically profile the chemical constituents of GGG roots, stems, and fruits, aiming to clarify the compositional characteristics of chemical components across different tissues [8]. Meanwhile, ultraviolet spectrophotometry was applied for the quantitative determination of total triterpenes and total tannins in these plant parts. Finally, in *vivo* pharmacodynamic experiments combined with Spearman correlation analysis were conducted to elucidate the correlations between chemical composition, constituent content, and pharmacological efficacy among different GGG tissues. Especially, this study integrated a comprehensive research system including constituent characterization, content quantification, pharmacodynamic validation, and key bioactive component analysis, constructing a targeted research framework to assess the feasibility of GGG stems as medicinal substitutes for GGG roots. This framework not only facilitates the systematic exploration of medicinal potential in underutilized plant tissues but also enriches ethnopharmacological research paradigms, offering a robust method for the systematic excavation of medicinal value from underexplored tissues in ethnic medicinal resources.

2. Materials and Methods

2.1. Plant Material

The roots, stems and fruits of GGG were collected from Qujing City, Yunnan Province, and were identified as the roots, stems and fruits of *Rosa odorata* Sweet var. *gigantea* (Coll. et Hemsl.) Rehd. et Wils., a medicinal herb of the Rosaceae family, identificated by Chen Yu of the Kunming Institute of Botany, Chinese Academy of Sciences. The sample specimens were stored at Tianjin Modern Innovation Chinese Medicine Technology Co., Ltd. (Tianjin, China).

2.2. Sample Preparation Methods

Three different parts (roots, fruits, stems) of *Rosa odorata* Sweet var. *gigantea* (Coll. et Hemsl.) Rehd. et Wils. were used. Dried powdered materials (500 g per part) were each reflux-extracted twice with 10 L (20:1 solvent-to-material ratio) of 60% ethanol solution for two hours per extraction. The resulting filtrates were combined and concentrated under reduced pressure. Subsequently, the concentrated extracts were spray-dried to obtain ROE (root extract, yield: 11.2% w/w), FOE (fruit extract, yield: 8.9% w/w), and SOE (stem extract, yield: 8.7% w/w).

2.3. UPLC-Q-TOF-MS Analysis

ROE, SOE, FOE were analyzed by UPLC-Q-TOF-MS. A high-performance liquid chromatography system (Waters, USA) was employed to analyze the compounds, and a CORTECS T3 column (2.1 mm×150 mm, 1.6μm) was used. The mobile phase used 0.1% formic acid in water as phase A and acetonitrile as phase B. The flow rate was set to 0.3 mL/min. The column temperature was set to 35 °C. The sample injection volume was set to 2 μL.

The proportion of the mobile phase was distributed over 110 min as follows: 0-12 min, 100%-97% A; 12-50 min, 97%-83% A; 50-60 min, 83%-66% A; 67-87 min, 55%-30% A; 87-106 min, 30%-20% A; 106-107 min, 20%-100% A; and 107-110 min, 100% A. UPLC-Q-TOF-MS was used to determine the charge-to-mass ratio of the compound, and the following positive and negative ion scanning modes were used to scan the range of m/z 100–1500: cone gas flow, 60 L/h; desolvation flow, 600 L/h; source temperature, 100 °C (positive)/100 °C (negative); desolvation temperature, 350 °C (positive)/350 °C (negative); cone voltage, 30 V (positive)/40 V (negative); and ion source voltage, 2.0 kV (positive)/3.0 kV (negative).

2.4. Multivariate Analysis

The raw spectra (raw data) were converted to mzML format using ProteoWizard software. The converted data were imported into the website (https://xcmsonline.scripps.edu), specific parameters were set, normalization was performed, etc., to obtain the data in different ion modes. The resulting data were collated in the MetaboAnalyst database (website http://www.metaboanalyst.ca) and used for principal component analysis (PCA).

2.5. GNPS Molecular Network Creation

Mass spectrometry analysis was performed according to the "2.2" detection conditions to obtain the raw files of UPLC-Q-TOF-MS secondary mass spectrometry of roots, stems and fruits under positive and negative ion modes. The original files were converted to 64-bit mzXML format files by MS Convert software, and then the mzXML files were imported after preprocessing by WinSCP software into GNPS (http://gnps.ucsd.edu) for data analysis. The specific parameter settings were set as follows: precursor ion mass tolerance (0.02 Da), fragment ion mass tolerance (0.05 Da), min pair cos (0.65), minimum number of matched fragment ions (6), and minimum cluster size (2). Visual analysis was performed with Cytoscape 3.9.1 (https://cytoscape.org/).

2.6. Methodology for Total Component Content Determination

2.6.1. Standard Solution Preparation

The reference substances of ursolic acid (ursolic acid (≥98.5%) was obtained from Macklin Inc. (China). U820325), gallic acid (gallic acid (≥99.0%) was obtained from Macklin Inc. (China). G823163) were accurately weighed, and the stock solution was prepared by dissolving and constant volume with methanol. Ursolic acid stock solution was diluted to 0.05, 0.10, 0.25, 0.50, 1.00, 1.50 mg/mL series concentration. The gallic acid stock solution was diluted to 0.175, 0.350, 0.700, 1.400, 2.800 mg/mL series concentrations.

2.6.2. Preparation of Test Solutions

The powders of root, stem and fruit (0.5 g ± 0.001 g, spray drying) was extracted with 20 mL 70% ethanol at 40 °C for 30 min, and the extraction was repeated once. The supernatant was combined and diluted to 50 mL. The sample solution was obtained by filtering through 0.45 μm filter membrane.

2.6.3. Colorimetric Method

Total triterpenoid chromogenic reaction: 1.0 mL of sample solution or ursolic acid standard solution was taken and dried in 70 °C water bath. 0.2 mL of 5% vanillin-glacial acetic acid solution and 0.8 mL of perchloric acid were added in turn. The reaction was carried out in 60 °C water bath for 20 min. After cooling in ice bath, 5 mL of glacial acetic acid was added and placed in the dark for 10min. The absorbance was measured at the wavelength of 553 nm, and the content of total

triterpenes (calculated as ursolic acid) was expressed according to the standard curve.

Chromogenic reaction for total tannins: A total of 1.0 mL test solution or gallic acid standard solution was added with 0.5 mL Folin-Ciocalteu reagent and 1.5 mL 10% Na_2CO_3 solution. The solution was diluted to 10 mL with distilled water and reacted in a water bath at 75 °C for 10 min. After cooling, the absorbance was measured at 760 nm. The total tannin content was calculated according to the standard curve (calculated as gallic acid).

A series of standard solutions of ursolic acid and gallic acid were treated by the above chromogenic method. The standard curve equation ($R^2>0.99$) was obtained by linear regression of concentration (X) to absorbance (Y), which was used to calculate the content of the test sample.

2.6.4. Spiking Recovery Test

Take an appropriate amount of a sample with a known content, like root extract. Accurately add a specific quantity of ursolic acid and gallic acid reference substances. Conduct the content determination according to the prescribed method. Calculate the spiking recovery rate. Perform three parallel determinations at each spiking level to validate the accuracy of the method.

2.7. Evaluation of Antidiarrheal Activity

2.7.1. Experimental Animal Husbandry

Male Kunming strain mice (24 ± 2 g) of specific pathogen-free (SPF) status were acclimated for 5 days under controlled environmental conditions (23 ± 3 °C, 60 ± 5% relative humidity) prior to experimental procedures. All animal protocols conformed to the Guidelines for the Care and Use of Laboratory Animals and were approved by the Institutional Animal Care and Use Committee of the Institute of Radiation Medicine, Tianjin Jinke Bona Biotechnology Co., LTD (GENINK-20250071).

Forty-two murine subjects were randomized into 6 experimental groups (n=7): control, model, berberine (100 mg/kg), ROE (500 mg/kg), SOE (500 mg/kg), FOE (500 mg/kg). Prior to experimentation, animals underwent 3-5 days acclimatization followed by 12-16 h fasting with ad libitum water access. On day 8, a castor oil-induced diarrhea model was established by intragastric administration of 0.2 mL ricinoleic acid-containing vehicle (0.1-0.2 mL/10 g optimized dose) to all groups except the blank control group. After a 24 h fasting period (water accessible), 5% activated charcoal suspension (0.1 mL/10 g, 0.2-0.3 mL/10 g optimized volume) was administered intragastrically. Cervical dislocation was performed 20 minutes post-charcoal administration (15-30 minutes observation window) to harvest intestinal segments from pylorus to ileum. The propulsive distance was measured and the propulsive rate of small intestine was calculated. The intestinal propulsion rate was calculated using the following formula:

$$\textbf{Intestinal propulsive rate (\%)} = \frac{\textbf{Carbon powder propulsion distance}}{\textbf{Total intestinal length}} \times 100\%$$

All parameters were optimized through preliminary trials to ensure experimental consistency.

2.7.2. Statistical Analysis

Data were analyzed using SPSS 22.0 software, expressed as mean ± standard deviation ($\bar{x}\pm s$), and evaluated by one-way analysis of variance (ANOVA). Statistical significance was defined as $^{*}P < 0.05$ and $^{**}P < 0.01$.

3. Results

3.1. UPLC-Q-TOF-MS Analysis of Different Parts of GGG

In this research, a UPLC-Q-TOF-MS approach was employed to perform qualitative analysis of the chemical compositions in the extracts from three distinct parts of GGG. By directly observing the base peak intensity (BPI) diagrams in positive and negative ion modes, it can be found that the chemical components of plant roots, stems and fruits are mainly manifested in the negative ion mode. After comparing the BPI diagrams, it was found that the roots and stems of GGG were similar to each other but different from the fruits.

Potential compounds in each extract were identified by integrating precise molecular weights, primary and secondary fragment ion peaks, and chemical composition data reported for congeneric plants.

Peak 6 is gallic acid (Fig.3A), showing a typical cleavage pathway in negative ion mode. Decarboxylation of (-CO_2) produces fragment ions at m/z 125.0239, and dehydration of (-H_2O) produces fragment ions at m/z 151.0031[9]. These characteristic cleavages allow rapid identification of gallic acid-derived parts in complex matrices [10]. Peaks 7, 8, 12, 21, 16, 13, etc. are analyzed according to this method.

Peak 44, identified as ellagic acid (Fig. 3C), followed dehydration (-H_2O) and decarboxylation (-CO_2) routes. Dehydration of ellagic acid (m/z 300.9995) gave a fragment at m/z 283.2965, and decarboxylation produced an ion at m/z 257.3327, serving as signature fragments for ellagic acid identification[11]. Peaks 14, 17, 30, 53 and other ellagic acid-derived compounds were also analyzed following this method.

Peak 59, identified as quercetin (Fig. 3B), exhibited diverse fragmentation pathways. It produced multiple diagnostic ions via retro-Diels-Alder (RDA) cleavages (e.g., $^{1,3}A^-$, $^{0,4}A^-$, $^{1,2}A^-$, $^{1,2}B^-$) and decarbonylation (-CO). For instance, $^{1,3}A^-$ cleavage yielded an ion at m/z 151.0117, while $^{1,2}A^-$ generated a fragment ion at m/z 178.9981, enabling differentiation of quercetin-type flavonoids from other polyphenols[12]. Peaks 37, 47, 48, 63 and other quercetin compounds were also analyzed in this way.

Peak 84, identified as oleanolic acid (Fig. 3D), showed stepwise cleavages involving formaldehyde (-HCHO), water (-H_2O), ethane (-C_2H_6), methane (-CH_4), and ethylene (-C_2H_4) losses. Initial loss of -HCHO/-H_2O from the parent ion (m/z 455.3506) formed m/z 407.1236, followed by sequential hydrocarbon losses to generate ions like m/z 377.2356, m/z 391.8736, and m/z 363.5669, which were pivotal for distinguishing oleanane-type triterpenoids[13]. Peaks 27, 28, 68, 71, 75 and other oleanolic acid-derived compounds were also analyzed following this method.

These fragmentation patterns, consistent with the fragmentation rules of natural products in the Rosaceae family, validated the reliability of our compound identification and reinforced the accuracy of GGG phytochemical profiling.

By analyzing the mass spectrometry peak. A total of 88 non-volatile chemical compounds were identified in the ROE, SOE, and FOE under negative ion mode, while 11 non-volatile compounds were potentially detected under positive ion mode. Detailed information on these compounds is provided in Figures 1,2,3 and Tables 1,2.

Subsequent analysis of the identified compounds showed that there was a high degree of chemical overlap between roots and stems, with 28 shared compounds. Among these shared compounds, there were 14 triterpenoids, accounting for 50%, and tannins and phenolic acids accounted for 32%. By identifying and counting all the identified compounds, it was found that the roots and stems had high similarity in the composition of compound types (Fig.4). It is worth noting that the triterpenoids identified in the stems were completely matched with the triterpenoids in the roots. From the perspective of chemical composition, stems can be used as potential medicinal substitutes for roots.

Table 1. Analysis of chemical constituents in extract of GGG in negative ion mode

NO.	RT/min	$[M-H]^-$	Secondary ion fragments	Molecular formula	Molecular name	ROE	SOE	FOE
1	1.25	191.0559	173.0098,127.0050	$C_7H_{12}O_6$	quinic acid	+	+	+
2	2.07	191.0191	111.0087,129.0183,173.0098,405.0270	$C_6H_8O_7$	isocitric acid	+	+	+
3	2.16	355.0324	191.0191,337.0209	$C_{14}H_{12}O_{11}$	chebulic acid	-	-	+
4	2.40	191.0191	111.0087,129.0206,173.0098	$C_6H_8O_7$	ocitric acid	+	-	+
5	4.01	481.0646	161.0446,293.0276,331.0666	$C_{20}H_{18}O_{14}$	3-O,4-O-(4,4',5,5',6,6'-hexahydroxybiphenyl-2,2'-diyldicarbonyl)-D-glucopyranose	+	+	+
6	5.14	169.0146	125.0236	$C_7H_6O_5$	gallic acid	+	+	+
7	5.62	331.0666	271.0436,191.0559,169.0146,429.0355,663.1401	$C_{13}H_{16}O_{10}$	1-O-galloyl-β-D-glucose	-	+	+
8	9.76	343.0662	169.0172,191.0559,483.0742	$C_{14}H_{16}O_{10}$	4-O-galloylquinic acid	-	+	-
9	11.81	153.0188	109.0306	$C_7H_6O_4$	2,4-dihydroxybenzoic acid	-	-	+
10	12.06	153.0188	109.0248,125.0213	$C_7H_6O_4$	protocatechuic acid	-	+	+
11	16.67	235.0249	191.0361,163.0387	$C_{11}H_8O_6$	2-(7,8-dihydroxy-2-oxochromen-4-yl) acetic acid	+	-	-
12	16.72	343.0662	-	$C_{14}H_{16}O_{10}$	3-galloylquinic acid	-	-	+
13	18.99	483.0788	162.0388,169.0172，325.0205，331.0666	$C_{22}H_{26}O_{12}$	4-hydroxy-2,6-dimethoxyphenol 1-O-β-D-(6'-O-gallonyl)-glucoside	-	+	-
14	19.04	633.0736	483.0742，211.0607	$C_{27}H_{22}O_{18}$	corilagin	+	+	-
15	19.10	325.0583	-	$C_{14}H_{14}O_9$	fertaric acid	-	-	+
16	21.66	345.0831	263.0729,483.0788	$C_{14}H_{18}O_{10}$	methyl 6-O-galloyl-β-d-glucopyranoside	+	+	+
17	23.14	633.0736	-	$C_{27}H_{22}O_{18}$	corilagin	+	+	-
18	23.38	633.0736	-	$C_{27}H_{22}O_{18}$	isocorilagin	+	+	-
19	23.93	633.0736	-	$C_{27}H_{22}O_{18}$	strictinin	-	-	+
20	26.98	577.1317	407.0777,289.0731,285.0383,245.0462,125.0259	$C_{30}H_{26}O_{12}$	procyanidin B3	+	-	-
21	27.90	495.0790	169.0146,191.0559,343.0662,593.0406,991.1588	$C_{21}H_{20}O_{14}$	3,4-di-O-galloylquinic acid	+	+	+
22	27.95	289.0696	577.1367,245.0815,203.0700,161.0264	$C_{15}H_{14}O_6$	epicatechin	+	+	-
23	28.84	321.0246	169.0119,125.0213	$C_{14}H_{10}O_9$	m-Galloylgallic acid	-	-	+
24	30.12	295.0079	251.0219,207.0314	$C_{12}H_8O_9$	2,3-dihydrobenzofuran-2,3,5,6-tetracarboxylic acid	+	-	-
25	30.51	495.0790	295.0079,251.0154,207.0314	$C_{21}H_{18}O_{14}$	gossypetin-8-glucuronide	+	+	+
26	31.92	291.0156	247.0248,203.0350,583.0302	$C_{13}H_8O_8$	brevifolincarboxylic acid	+	+	+
27	33.67	603.0708	453.1031,1207.1544	$C_{35}H_{56}O_8$	hederagenin 3-O-arabinoside	+	+	-
28	33.82	197.0459	169.0146	$C_9H_{10}O_5$	methyl 3-O-methyl gallate	+	+	+
29	34.29	935.0771	197.0459,467.0389	$C_{41}H28O_{26}$	stachyurin	-	+	-
30	35.45	785.0823	289.0696,631.0504	$C_{34}H_{26}O_{22}$	tellimagrandin I	-	+	-
31	35.86	289.0696	579.1504,441.0152,245.0815,137.0259,125.0259	$C_{15}H_{14}O_6$	catechin	+	+	-
32	37.05	633.0736	731.0405,1267.1530	$C_{27}H_{22}O_{18}$	isostrictinin	+	+	+
33	38.20	247.0248	207.0311,495.0562	$C_{12}H_8O_6$	brevifolin	+	+	-
34	38.96	635.0276	169.0146,293.0276,465.0674,671.0574	$C_{27}H_{24}O_{18}$	3-di-galloyl glucoside-4,5-dihydroxybenzoic acid	-	-	+
35	39.95	561.1384	289.0766,659.1018	$C_{30}H_{26}O_{11}$	ent-fisetinidol-(4β→6)-catechin	+	-	-
36	40.93	729.1498	577.1415,169.0092	$C_{37}H_{29}O_{15}$	3-O-galloylprocyanidin B3	+	-	-
37	41.51	625.1385	303.0848,347.0753,475.0428,661.1385	$C_{27}H_{30}O_{17}$	quercetin-7-O-β-gentobioside	-	+	-
38	42.38	935.0771	303.0153,277.0363,259.0261,231.0336,171.0309	$C_{34}H_{24}O_{22}$	iso-oenothein C	-	-	+
39	42.47	561.1384	409.0922,289.0731,203.0729	$C_{30}H_{26}O_{11}$	fisetinol-(4β-8)-catechin	+	+	-
40	43.66	561.1384	435.1100, 407.0760, 289.0701	$C_{30}H_{26}O_{10}$	(-)-afzelechin-(4α→8)-epicatechin	+	+	-
41	44.49	497.1269	401.1543,561.1384	$C_{22}H_{23}O_{11}$	peonidin 3-glucoside	+	-	-
42	45.59	609.1455	491.0459	$C_{27}H_{30}O_{16}$	quercetin 3-rutinoside	-	+	-
43	47.08	319.0464	273.0025,245.0078,189.0206,191.0415	$C_{15}H_{12}O_8$	dihydromyricetin	+	+	-
44	47.33	300.9995	603.0054,257.3327	$C_{14}H_6O_8$	ellagic acid	+	+	+
45	47.91	561.1384	433.0402,409.0963,300.9959	$C_{30}H_{26}O_{11}$	phaeosphaerin E	+	-	-
46	48.47	545.1450	493.1991,433.0445,300.9994,180.9142	$C_{30}H_{26}O_{10}$	-	+	-	-
47	48.90	477.0668	303.0509	$C_{21}H_{18}O_{13}$	quercetin-3-O-glucuronide	-	+	-
48	49.40	463.0867	303.0509,301.0385,252.0689,	$C_{21}H_{20}O_{12}$	isoquercitrin	-	+	-
49	51.57	477.1025	409.0789,365.0840,303.0207	$C_{22}H_{22}O_{12}$	nepetin-7-glucoside	-	+	-
50	51.75	579.1356	477.0936, 319.0428	$C_{26}H_{28}O_{15}$	kaempferol 3-[apiosyl-(1→2)-galactoside	-	+	-
51	53.60	425.0157	327.0364,300.9994,851.0333	$C_{20}H_{10}O_{11}$	1'-monodecarboxyvaloneic acid dilactone	-	+	-
52	53.92	461.0707	285.0383, 257.0499,229.0517	$C_{21}H_{18}O_{12}$	kaempferol-3-glucuronide	-	+	-
53	54.17	447.0560	315.0140,250.9019,221.0802,179.0681	$C_{21}H_{18}O_{12}$	methylellagicacid 4'-O-β-D-arabinopyranosi-de	+	-	-
54	56.14	613.0837	425.0114,711.0485	$C_{28}H_{22}O_{16}$	6-[5,7-dihydroxy-2-(4-hydroxyphenyl)-4-oxochromen-3-yl]oxy-3,4-dihydroxy-5-(3,4,5-trihydroxybenzoyl)oxyoxane-2-carboxylic acid	-	+	-
55	56.55	349.0581	447.0214,197.0459,169.0146	$C_{16}H_{14}O_9$	ethyl 3,4-dihydroxy-5-[(3,4,5-trihydroxybenzoyl)oxy]-β-enzoate	-	-	+
56	56.90	497.0310	498.0358,995.0823	$C_{32}H_{50}O_4$	3-β-O-acetylbetulinic acid	+	-	+
57	58.47	711.3925	503.3325,549.3412,1377.8000	-	-	+	+	-
58	58.98	519.3346	-	$C_{30}H_{48}O_7$	16α-hydroxyprotobassic acid	+	-	-
59	59.02	301.0350	273.0396,178.9981,121.0912,151.0117	$C_{15}H_{10}O_7$	quercetin	+	+	-
60	59.96	593.1303	503.3417,423.0002,301.0030	$C_{30}H_{26}O_{13}$	tiliroside	+	+	+
61	60.32	709.3786	501.3223,547.3226,761.3449	-	-	+	-	-

Table 1 (continued)

62	61.95	695.399	487.3412,747.3636,1345.8138	-	-	+	+	+
63	62.08	285.0383	301.0736,255.0250,135.0735	$C_{15}H_{10}O_6$	5-desoxyquercetin	+	+	-
64	67.34	503.3371	549.3412,485.3317,623.2763,1007.6855	$C_{30}H_{48}O_6$	madecassic acid	+	+	+
65	69.22	517.3159	518.3177，180.9115	$C_{30}H_{46}O_7$	jaligonic acid	+	+	+
66	69.66	517.3159	455.3113,439.2881,180.9170	$C_{30}H_{46}O_7$	vismiaefolic acid	+	-	+
67	69.86	487.3412	533.3431,485.3227,311.2239	$C_{30}H_{48}O_5$	euscaphic acid	-	-	+
68	71.43	487.3412	215.1650,533.3478,555.3759,607.2820	$C_{30}H_{48}O_5$	asiatic acid	-	-	+
69	71.63	487.3412	533.3478,555.3759,607.2820，975.6896	$C_{30}H_{48}O_5$	acuminatic acid	+	+	+
70	73.16	501.3223	487.3503,547.3273	$C_{30}H_{46}O_6$	16α-hydroxygypsogenic acid	+	+	-
71	76.27	485.3272	531.3305,467.3133	$C_{30}H_{46}O_5$	quinovic acid	+	+	+
72	76.43	485.3272	531.3305,467.3133	$C_{30}H_{46}O_5$	gypsogenic acid	+	+	-
73	77.58	269.1523	135.0389,133.0593,119.0164	$C_{18}H_{22}O_2$	hexestrol	-	-	+
74	77.92	431.2184	-	$C_{28}H_{34}O_4$	23-oxo-isotingenone	-	-	+
75	79.17	471.3458	455.3156,401.2240,311.1697	$C_{30}H_{48}O_4$	maslinic acid	+	-	+
76	79.27	483.3083	465.2970,	$C_{31}H_{48}O_4$	methyl glycyrrhetinate	+	+	-
77	80.37	471.3458	311.1661,517.3532	C30H48O4	hederagenin	-	-	+
78	81.54	433.2363	-	$C_{28}H_{34}O_4$	6-Oxotingenone	+	+	+
79	81.71	663.3879	433.2320,353.2021,313.2357	$C_{40}H_{56}O_8$	2α,19-dihydroxy-3β-[[(E)-3-(4-hydroxy-3-methoxyphenyl)propenoyl]oxy]urs-12-ene-28-oic acid	+	+	-
80	82.48	483.2723	433.2363	$C_{29}H_{40}O_6$	ethyl lucidenate F	+	+	+
81	85.85	633.3776	669.3558,691.3443	-	-	+	-	-
82	89.03	277.2173	-	$C_{18}H_{30}O_2$	linolelaidic acid	+	+	+
83	89.10	277.2173	259.0399,180.9115,116.9280	$C_{18}H_{30}O_2$	γ-linolenic acid	-	-	+
84	89.54	455.3506	377.2356,391.8736,501.3590,575.2934	$C_{30}H_{48}O_3$	oleanolic acid	+	+	+
85	90.36	647.3943	455.3506,473.3618,1295.7992	$C_{36}H_{56}O_{10}$	2α,3α,24-trihydroxyurs-12,18-dien-28-oic acid β-D-glucopyranosyl ester	+	-	-
86	90.44	473.3618	323.2591,455.3550,647.3943	$C_{30}H_{50}O_4$	soyasapogenol A	+	-	-
87	93.41	279.2325	339.2311,877.6596	$C_{18}H_{32}O_2$	linoleic acid	+	+	+
88	103.83	497.3643	565.3517	$C_{32}H_{50}O_4$	β-boswellic acid acetate	+	-	-

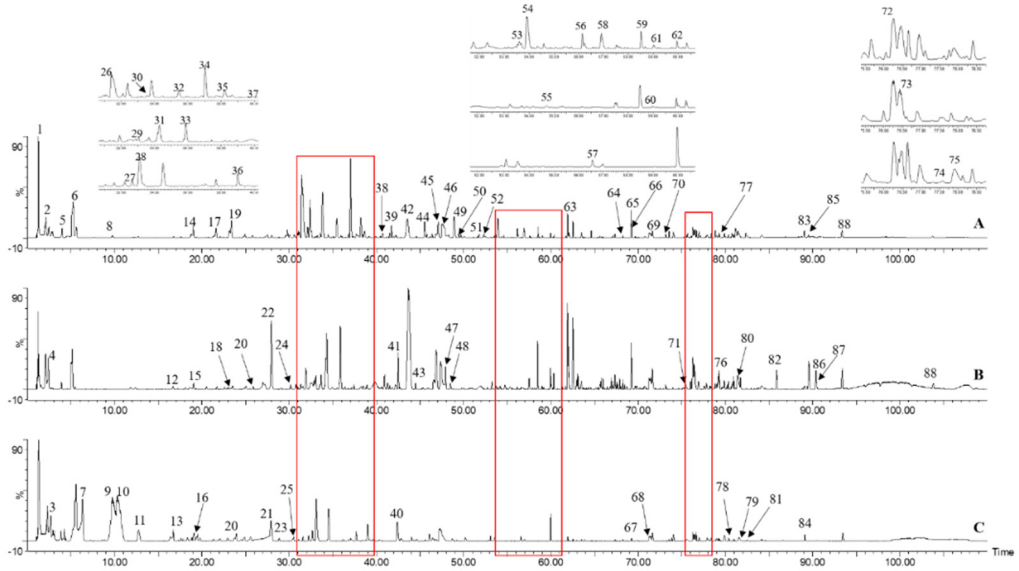

Figure 1. Ion flow diagram of *Rosa odorata* Sweet var. *gigantea* (Coll. et Hemsl.) Rehd. et Wils. roots, stems and fruits in negative ion mode. A: BPI of SOE in negative ion mode. B: BPI of ROE in negative ion mode. C: BPI of FOE in negative ion mode.

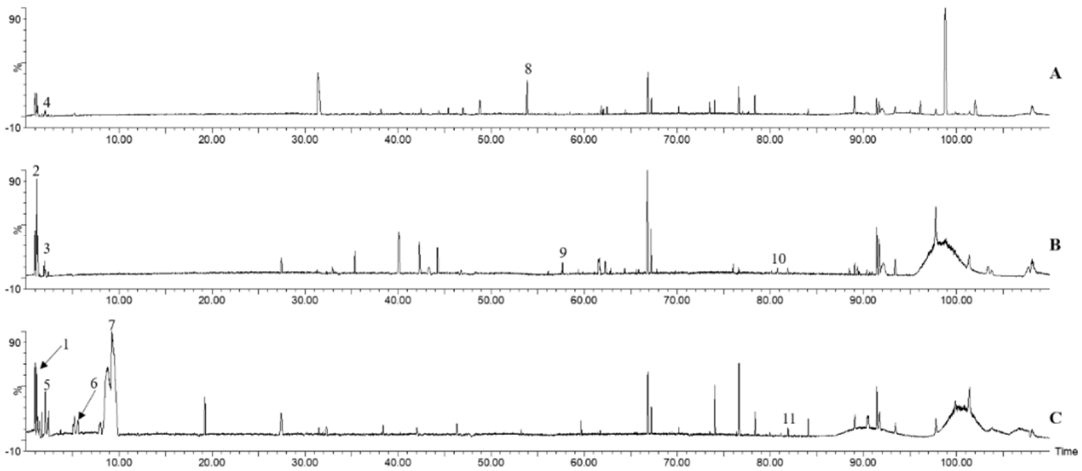

Figure 2. Ion flow diagram of *Rosa odorata* Sweet var. *gigantea* (Coll. et Hemsl.) Rehd. et Wils. roots, stems and fruits in positive ion mode. Ion flow diagram of *Rosa odorata* Sweet var. *gigantea* (Coll. et Hemsl.) Rehd. et Wils. roots, stems and fruits in positive ion mode. A: BPI of SOEs in positive ion mode. B: BPI of ROE in positive ion mode. C: BPI of FOE in positive ion mode.

Table 2. Analysis of chemical constituents in extract of GGG in positive ion mode

No.	RT/min	$[M+H]^+$	secondary ion fragments	molecular formula	molecular name	ROE	SOE	FOE
1	1.16	209.0268	203.0522,133.0620	$C_{11}H_6O_5$	(E)-2-carboxybenzylidenepyruvate	-	-	+
2	1.21	266.1248	248.1145,203.0522,179.0628,138.0553	$C_{14}H_{18}O_5$	ethyl 2,4,6-trimethoxycinnamate	+	-	-
3	1.98	146.0933	-	$C_5H_{11}N_3O_2$	hlycyl-N-methylglycinamide	+	-	-
4	2.08	215.0147	-	$C_8H_6O_7$	2,4,6-Trihydroxy-1,3-benzenedicarboxylic acid	-	+	-
5	2.09	215.0177	189.0050,175.0252	$C_8H_6O_7$	5-hydroxy-6-methoxycarbonyl-4-oxo-pyran-2-carboxylic acid	-	-	+
6	5.65	355.0440	171.0283	$C_{15}H_{14}O_{10}$	2-O-p-coumaroylhydroxycitric acid	-	-	+
7	9.26	345.0837	367.0666,327.0722,171.0194	$C_{14}H_{16}O_{10}$	1,3,4-trihydroxy-5-(3,4,5-trihydroxybenzoyl) oxycyclohexane-1-carboxylic acid	-	-	+
8	57.68	505.3535	469.3308,373.6942	$C_{30}H_{50}O_6$	theasapogenol A	+	-	-
9	80.78	317.2079	277.2168,187.6039	$C_{20}H_{28}O_3$	2-methoxyestradiol-3-methylether	+	-	-
10	81.89	301.1411	363.1193	$C_{18}H_{20}O_4$	5,7,4'-trimethoxyflavan	-	-	+
11	89.09	317.1788	-	$C_{19}H_{26}O_4$	2-methoxyestriol	-	-	+

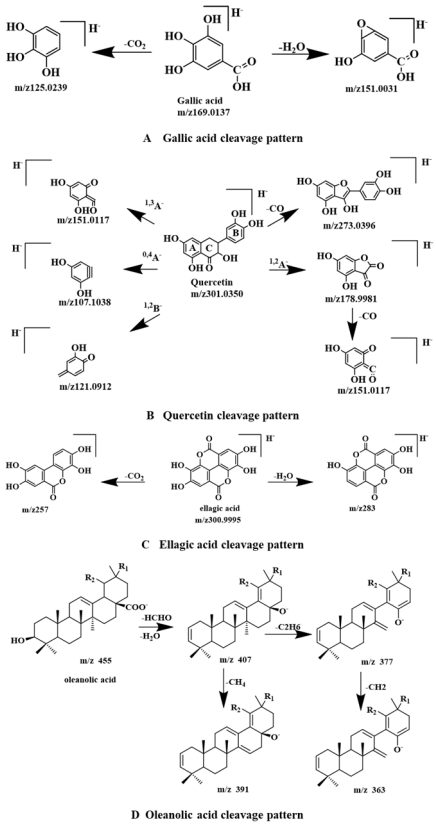

Figure 3. Cracking mode of some compounds

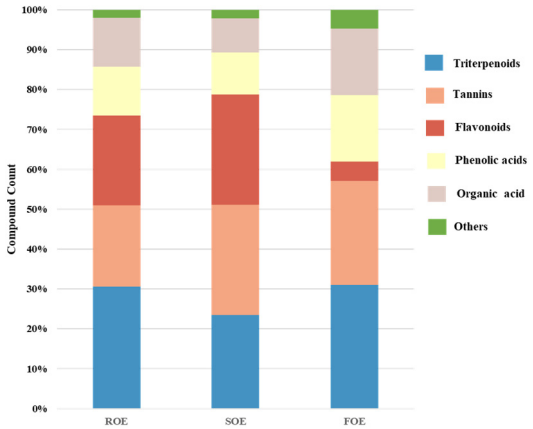

Figure 4. Distribution proportion map of UPLC-Q-TOF-MS identified components in different parts of GGG

3.2. Identification of the Chemical Composition and Creation of a Molecular Network Using GNPS

In order to further verify the structural annotation of the identified compounds and intuitively characterize the clustering relationship of chemical components among different tissues, the Global Natural Products Social Molecular Networking (GNPS) technology was used to construct a visual network. The GNPS serves as a global open- access platform for processing mass spectrometry data, facilitating the visualization and structural annotation of molecular structures [14]. Molecular network technology constructs molecular networks by conducting similarity analyses on secondary mass spectra[15]. During this procedure, natural products with similar structures, when subjected to identical mass spectrometry cleavage conditions, will generate comparable characteristic fragment ions[15]. Subsequently, the computer matches the similarity of these fragment ions and generates a visual network diagram based on the magnitude of their similarity (cosine value)[16]. Each node in the diagram represents the mass spectrometry-related information of a compound, and compounds with similar and dissimilar structures are clustered into different molecular networks [17].

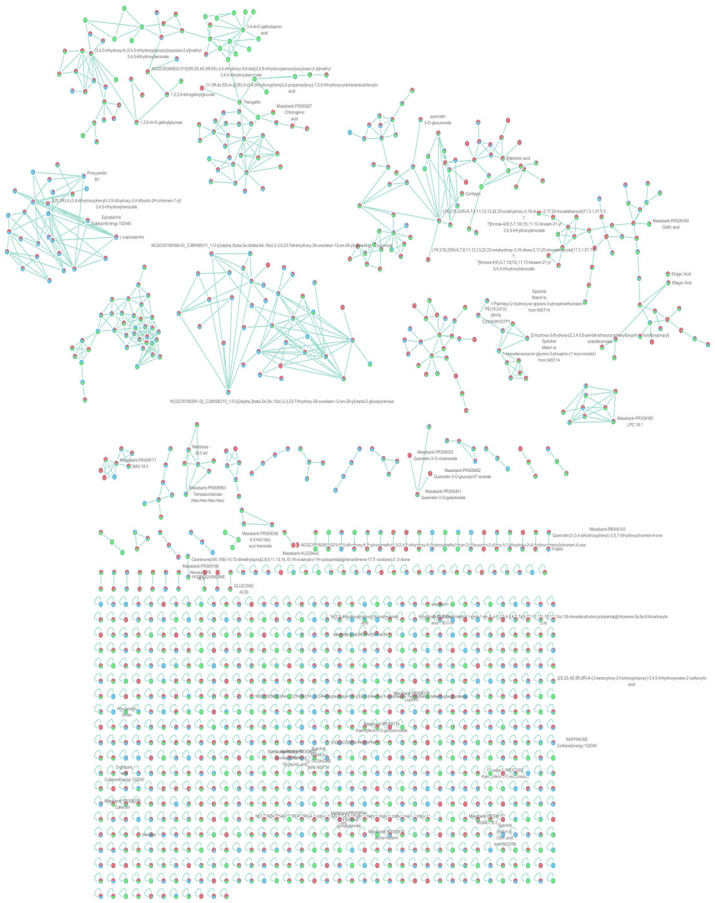

Figure 5. Molecular network diagram for GNPS visualization of roots, stems and fruits red: ROE; blue: SOE; green: FOE

The mass spectrometry data of the roots, stems and fruits were processed via the GNPS website to generate a visual molecular network diagram that interconnected these components. As depicted in figure 5, GNPS discriminates the chemical compositions among the compounds based on the degree of similarity between them, links the compounds, and simultaneously matches the compound information stored in the GNPS database[18]. In this study, a total of 35 compounds' information was retrieved through the GNPS database. These compounds encompass flavonoids (such as quercetin-3-O-rutinoside and kaempferol-3-O-glucuronoside), phenolic acids (e.g., 3,4-di-O-galloylquinic acid), tannins (e.g.,1,3,6-tri-O-galloylglucose, ellagic acid), triterpenoids (specifically β-D-Glucopyranosyl (2α,3β,5α,9β,18α)-2,3,23-trihydroxy-28-oxoolean-12-en-28-oate), steroids, organic acids (for instance, citric acid), and fatty acids, among others.

Beyond compound identification via database matching, the molecular network visualization results further revealed the distribution patterns of these components across different tissues and their structural correlations[19]. Based on the visualization results of the molecular network, it can be observed that diverse chemical components are mainly distributed in molecular networks with more than 5 network nodes. In addition, the content of specific chemical components can be inferred from the change of node color. Taking a molecular network node as an example (Fig 6. A), it mainly shows the connection of tannin components in roots and fruits, representing that substances like gallic acid tannins are mainly distributed in roots and fruits. Several solid green nodes presented in the figure indicate that the corresponding chemical components only exist in fruits. For the interrelated chemical components in roots and stems, they are mainly a class of triterpenoid saponins with oleanolic acid as the

aglycone. As shown in Fig. 6B, this type of chemical components is mainly found in stems and roots[20].

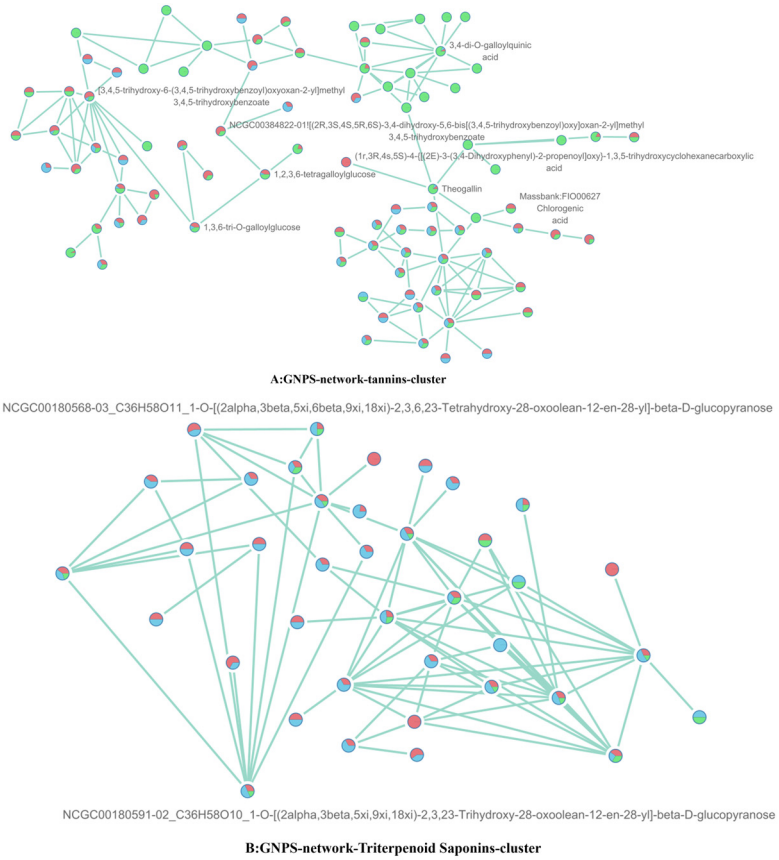

Figure 6. Partial molecular network node diagram red: ROE; blue: SOE; green: FOE

Overall, the chemical components shown in the GNPS molecular network are mainly phenolic acids, tannins, triterpenoids, and flavonoid glycosides. The unique chemical component type in roots is acetylated triterpenoids, and the unique type in stems is malonyl flavonoid glycosides. The proportion of cross-tissue shared nodes between roots and stems accounts for 28% of all nodes, while that between roots and fruits accounts for 13%, indicating that stems have a greater chemical correlation with roots compared to fruits. Notably, the number of isolated nodes in roots is the highest among the three parts, suggesting that roots may contain various chemical components that have not yet been identified. In these unrecognized isolated nodes, both blue and red are contained, that is, the components shared by roots and stems account for about 65 %, which can also reflect that roots and stems are relatively similar in chemical composition.

3.3. PCA Analysis of GGG Root, Stem and Fruit

In order to further confirm the similarity of chemical constituents between roots and stems, PCA analysis was performed on the extracts of roots, stems and fruits. Principal component analysis (PCA) revealed distinct clustering patterns among the root (ROE), stem (SOE), and fruit (FOE) extracts. The scores plot demonstrated a high similarity between the chemical profiles of ROE and SOE, as evidenced by their adjacent and overlapping clusters. Conversely, the FOE profile was markedly separated from the root and stem clusters, indicating a significant chemical divergence of the fruit from the other plant parts (Figure 7). This result further confirms that the stem can be used as a potential medicinal part of the root.

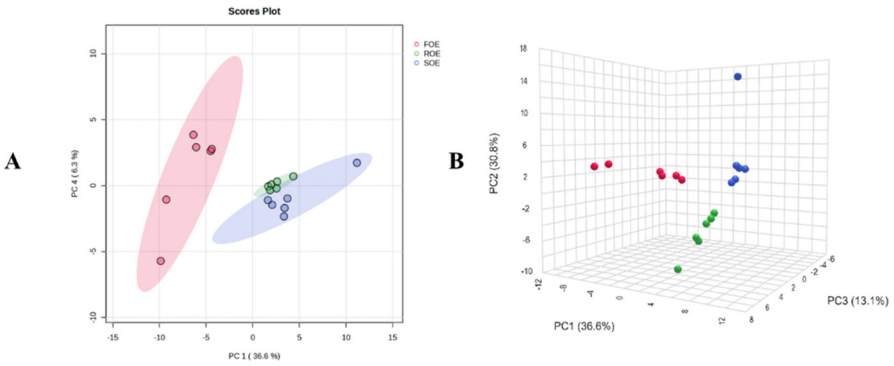

Figure 7. ROE, SOE, and FOE principal component analysis difference plots.
A. Negative ion mode 2D; B. Negative ion mode 3D.

3.4. Quantitative Results of Total Components

Total triterpenes and total tannins were quantified via ultraviolet (UV) spectrophotometry, with ursolic acid and gallic acid selected as reference standards, respectively, due to their structural representativeness in triterpenoids and tannins. Briefly, serial concentrations of ursolic acid (0.02-0.10 mg/mL) and gallic acid (0.01-0.05 mg/mL) standard solutions were prepared to construct calibration curves. The absorbances were measured at 546 nm (for total triterpenes) and 760 nm (for total tannins), and the regression equations exhibited correlation coefficients $R^2 > 0.999$, confirming good linearity. For sample analysis, dried extracts of GGG roots, stems, and fruits were precisely weighed, dissolved in methanol, subjected to ultrasonic extraction (40 kHz, 30 min), and centrifuged (8000 rpm, 10 min) to obtain clear supernatants. After appropriate dilution to fit the linear range of the calibration curves, the absorbances of samples were determined under the same conditions as the standards. The quantitative results showed that the total triterpene contents of the roots, stems and fruits were 21.77%, 19.24% and 23.86%, respectively, while the total tannin contents were 55.84%, 56.77% and 53.57%, respectively. Comparative analysis revealed that the contents of these two main bioactive components in stems were close to those in roots, further supporting the potential of stems as an alternative medicinal part to roots.

3.5. Comparison of Antidiarrheal Activity

To evaluate the antidiarrheal activity of GGG stems, this study employed a castor oil-induced murine diarrhea model, with berberine serving as the positive control. The intestinal propulsion distance was measured following intervention with total extracts from the ROE, SOE, and FOE.

As summarized in Figure 8, all extract groups exhibited significantly lower intestinal propulsion rates compared to the model control group ($P< 0.01$). Crucially, intestinal motility inversely correlated with antidiarrheal efficacy: a reduced propulsion rate indicated enhanced suppression of intestinal peristalsis, thereby demonstrating superior antidiarrheal effects.

Compared to the blank control group, the intestinal propulsion rate was significantly elevated in the model group (64.8±5.6%, $P< 0.01$), confirming the successful establishment of the diarrhea model. Treatment with both root extract (ROE) and stem extract (SOE) markedly inhibited this hypermotility, yielding propulsion rates of 42.3±7.5% and 41.1±3.4%, respectively. These values were significantly lower than that of the model group (64.8±2.8%, $P< 0.01$ for both comparisons) and were comparable to the efficacy observed in the positive control drug group. In contrast, the FOE demonstrated a moderate effect, with a propulsion rate of 47.4±5.5%, which was higher than that of both ROE and SOE yet still significantly lower than the model group ($P< 0.05$). The results showed that GGG root, stem and fruit had antidiarrheal effect, and the effect of root and stem was similar and better than that of fruit.

To further elucidate the intrinsic correlations among chemical constituents, contents, and pharmacological effects in GGG roots, stems, and fruits, and clarify the differential characteristics across these tissues, a Spearman's correlation heatmap (Fig. 9) was constructed[21]. This analysis focused on the associations between 82 identified compounds (designated as X1-X82) and intestinal propulsion rate (TJL), a key indicator reflecting antidiarrheal activity. Correlation strength was characterized by color intensity and Spearman's correlation coefficient (r, range: -1.0 to 1.0). "Spearman's rank correlation coefficient"[22]: a negative correlation (blue color) indicated that higher compound content correlated with lower TJL (stronger antidiarrheal activity), while a positive correlation (red color) indicated higher compound content correlated with higher TJL (weaker antidiarrheal activity). Correlation strength was defined as: weak ($|r| < 0.25$), moderate ($0.25 \leq |r| < 0.5$), and strong ($|r| \geq 0.5$)[23]. Statistical significance was marked with asterisks following standard academic conventions: $^{***}P < 0.001$, $^{**}P < 0.01$, $^{*}P < 0.05$, and no asterisk indicated $P \geq 0.05$[24]. Key findings are summarized as follows: Triterpenoids and partial tannins exhibited strong and significant negative correlations with TJL ($r<-0.5$), indicating they are core antidiarrheal active constituents. Representative compounds included procyanidin B3 (X19), isocorilagin (X17), corilagin (X14), acuminatic acid (X64), methyl glycyrrhetinate (X71), 16α-hydroxygypsogenic acid (X65), and soyasapogenol A (X80). Notably, typical triterpenoids such as hederagenin (X72) and oleanolic acid (X35) maintained stable negative correlations, consistent with their reported anti-inflammatory and gastrointestinal mucosal protective effects.

Tannins and phenolic acids showed differential correlations: isocitric acid (X2) and gallic acid (X6) exhibited significant negative correlations with TJL, further confirming the contribution of tannins/phenolic acids to antidiarrheal activity. In contrast, protocatechuic acid (X10) displayed a moderate positive correlation ($r\approx 0.3$-0.4^{*}), suggesting a secondary regulatory role in intestinal motility.

Most flavonoids (e.g., dihydromyricetin, X43) showed weak correlations ($|r| < 0.25$) or no significant correlations with TJL, indicating their limited direct effect on regulating intestinal propulsion rate. Additionally, multiple compounds including organic acids (e.g., isocitrate, X2) showed no significant correlations with TJL, implying they are not the key contributors to antidiarrheal activity.

Further analysis was conducted on the main components negatively correlated with the small intestinal propulsion rate in roots and stems. The top 10 compounds with the most negative correlation coefficients in each part were selected, and the results are presented in the Venn diagram (Fig. 10). It can be observed that the main compounds exerting effects in both roots and stems are primarily triterpenoids and tannins. Moreover, notably, most of the key active compounds are shared between roots and stems. Combined with the above Spearman correlation heat map results and previous component analysis data, it can be seen that the key medicinal components (mainly triterpenes and tannins) of GGG roots and stems are highly overlapped. This finding indicates that the stem has the potential to be used as a root alternative medicinal part, regardless of the chemical composition or the type and activity of the core bioactive components.

4. Discussion

As a traditional medicinal plant of the Yi nationality in China, GGG, with its significant astringent, anti-inflammatory and anti-diarrheal properties. It has long been used in the traditional medical practice of the Yi nationality for intervening in diseases such as dysentery, diarrhea, and

gastrointestinal disorders[1]. Modern pharmacological studies have further validated the core medicinal value of its roots, and the efficacy of this plant part has been widely recognized in clinical research[25]. Its fruits are rich in bioactive nutritional components and exhibit both medicinal and edible properties, indicating promising prospects for resource development.

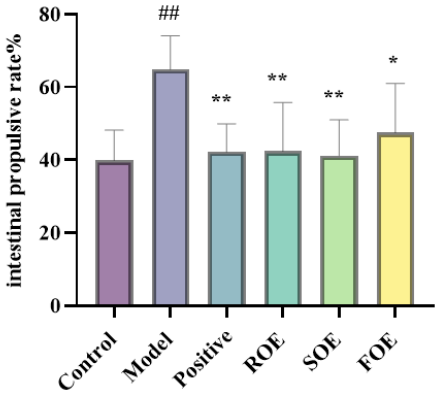

Figure 8. Effects of different parts of GGG on intestinal advancement rate in castor oil-induced diarrheic mice ($\bar{x} \pm s$)
##P<0.01 compared with the control group; *P<0.05, **P<0.01 compared with the model group

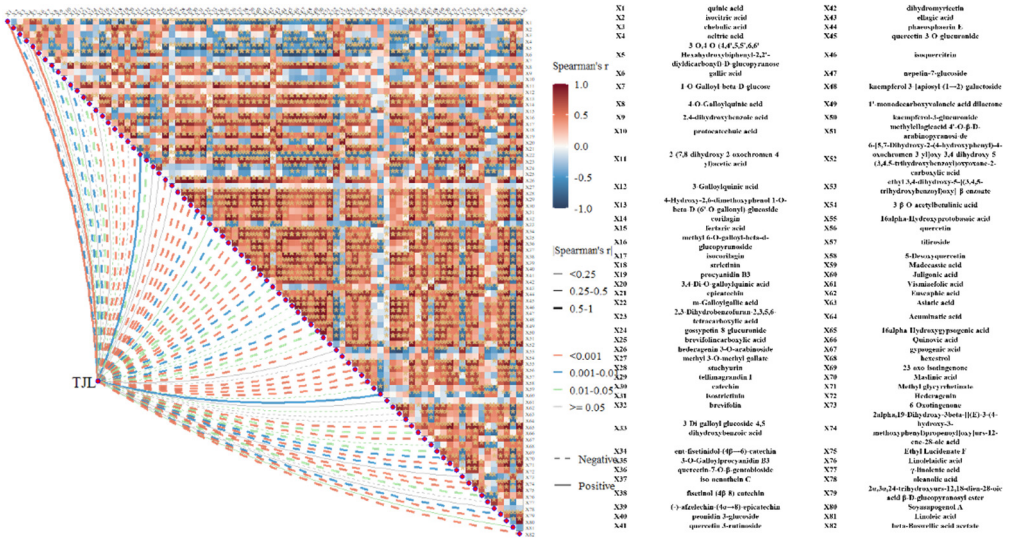

Figure 9. Correlational study on phytochemicals from organ-specific GGG and intestinal propulsion rate

However, against the backdrop of the growing demand for the sustainable utilization of ethnic medicinal resources in China[26] and the deepening exploration of the medicinal value of multiple plant parts, two core questions urgently need clarification: first, whether the large quantities of discarded stem and branch resources generated during root harvesting possess reuse value; second, whether GGG stems can serve as a potential alternative medicinal part to roots, thereby overcoming the limitation of resource utilization that "relies solely on roots and fruits" and enabling the efficient development of whole-plant resources. To address these needs, this study systematically compared and analyzed the chemical constituents and pharmacological activities of GGG roots, stems, and fruits, providing key scientific support for the comprehensive development and utilization of this plant resource.

To clarify the relationships among the chemical compositions of GGG roots, stems, and fruits, this study established a comprehensive analytical system integrating multiple technologies from a qualitative perspective. First, UPLC-Q-TOF-MS was employed to analyze the components of ROE, SOE, and FOE under positive and negative ion scanning modes (m/z 100–1500). The analysis integrated accurate molecular weights, primary and secondary fragment ion characteristics (e.g., m/z 125.0239: decarboxylation fragment of gallic acid; m/z 407.1236: dehydration-formaldehyde fragment of oleanolic acid), and databases of known Rosaceae plant components, leading to the identification of 28 common non-volatile compounds. Furthermore, GNPS molecular networking analysis was performed to construct a clustering network based on fragment ion similarity (*cos*≥0.65). The results revealed that triterpenoids (e.g., oleanolic acid, hederagenin) and tannins (e.g., corilagin, isocorilagin) in roots and stems formed highly overlapping node clusters. Specifically, all 11 triterpenoids identified in stems completely overlapped with 15 triterpenoids in roots, with a tannin overlap rate exceeding 85 %. These findings indicate a high degree of consistency in the structure and category of key bioactive components between roots and stems. Concurrently, PCA results demonstrated that the chemical profile clusters of ROE and SOE in negative ion mode were closely aligned and partially overlapping—distinct from the discrete clustering of FOE. This further confirmed the similarity in chemical composition between roots and stems at the overall chemical characteristic level.

In addition, regarding efficacy experiments, the anti-diarrheal activity of extracts from different GGG parts (roots,

stems, fruits) was evaluated using a castor oil-induced mouse diarrhea model, and the pharmacodynamic material basis was analyzed via Spearman correlation analysis. The results demonstrated that the pharmacological effects of ROE and SOE were highly similar but distinct from those of FOE. Specifically, the intestinal propulsion rate of mice in the model group was 64.8 ± 5.6 %, while after intervention, ROE and SOE reduced this rate to 42.3 ± 7.5 % and 41.1 ± 3.4 % (both $P<0.01$), respectively. The inhibitory effects of ROE and SOE on excessive intestinal peristalsis were comparable and close to that of the positive control (berberine). In contrast, FOE intervention resulted in a propulsion rate of 47.4 ± 5.5 % ($P<0.05$), with significantly weaker anti-diarrheal activity than ROE and SOE.

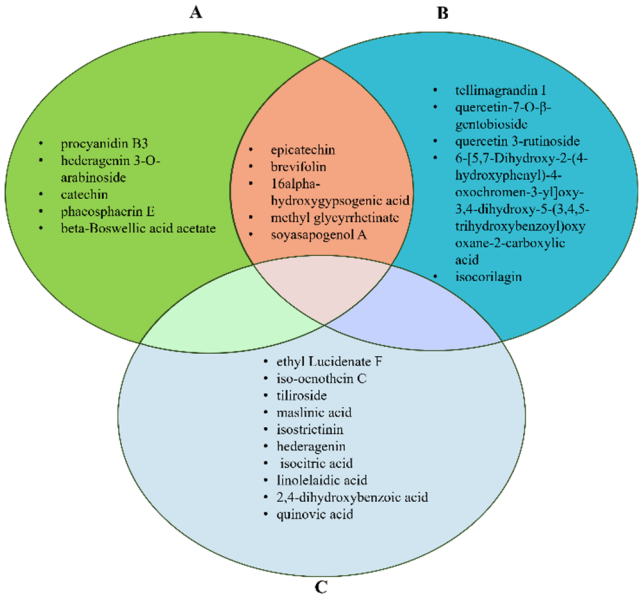

Figure 10. Integrated analysis of bioactivity, key compound distribution, and total content correlation in different plant parts
A Top 10 compounds in ROE showing negative correlation with intestinal propulsive rate
B Top 10 compounds in SOE showing negative correlation with intestinal propulsive rate
C Top 10 compounds in FOE showing negative correlation with intestinal propulsive rate

These data indicate that GGG roots and stems exhibit similar and stronger anti-diarrheal effects. Combined pharmacodynamic substance analysis further clarified that among the 88 compounds identified in negative ion mode, 23 components were significantly negatively correlated with intestinal propulsion rate ($r<-0.3$, $P<0.05$), and these components are the main contributors to anti-diarrheal activity. The top 10 components with the strongest correlation to the anti-diarrheal efficacy of each plant part were selected for distribution analysis. This analysis revealed that these core bioactive components are predominantly concentrated in triterpenoids (e.g., 16α-hydroxyglycyrrhetinic acid, methyl glycyrrhetinate, soyasaponin A) and tannins (e.g., epicatechin, brevifolin), accounting for over 80% of the top 10 components. Notably, 5 components were common to the top 10 lists of roots and stems: epicatechin, brevifolin, 16α-hydroxyglycyrrhetinic acid, methyl glycyrrhetinate, and soyasaponin A. This finding further confirms a high degree of overlap in the composition of bioactive substances between roots and stems.

Literature evidence clearly supports the anti-inflammatory and anti-diarrheal activities of these 5 common components. For instance, epicatechin — a typical tannin component[27, 28] — can alleviate inflammatory damage to the intestinal mucosa by enhancing the integrity of intestinal epithelial tight junctions and inhibiting the activation of the NF-κB inflammatory pathway[29, 30]. Brevifolin (previously referred to as "short-leaf xylenol") exerts anti-inflammatory and intestinal protective effects by scavenging intestinal reactive oxygen species (ROS) and regulating the M1/M2 polarization balance of macrophages[31]. As an oleanolic acid-type triterpenoid, 16α-hydroxygypsogenic acid inhibits excessive contraction of intestinal smooth muscle, downregulates the expression of pro-inflammatory cytokines (e.g., IL-1β, TNF-α), and alleviates diarrhea symptoms[32]; methyl glycyrrhetinate activates glucocorticoid receptors, inhibits intestinal inflammation, and regulates gut microbiota composition, with its anti-diarrheal activity validated in multiple animal models[33]; soyasaponin A synergistically enhances anti-diarrheal efficacy by inhibiting the adhesion of intestinal pathogenic bacteria (e.g., Salmonella) and improving intestinal barrier function[34]. Collectively, these studies demonstrate that the five core components shared by GGG roots and stems possess distinct anti-inflammatory and anti-diarrheal mechanisms and are concurrently enriched in both tissues. This further confirms, from the perspective of the mechanism of pharmacodynamic substances, that roots and stems exert comparable pharmacological contributions—providing a key pharmacodynamic basis for stems to serve as an alternative medicinal part to roots.

Based on the aforementioned qualitative analysis, quantitative determination, and pharmacodynamic validation results, GGG stems and roots exhibit a high degree of consistency in chemical composition and pharmacological activity. Specifically, GGG stems closely align with roots in terms of chemical composition, bioactive component content, and pharmacological efficacy, highlighting their potential as an alternative medicinal part to roots. Concurrently, this study establishes a technical framework for the development of whole-plant resources of Rosaceae medicinal plants. It not only addresses the long-standing issue of GGG stem resource waste but also provides scientific support for the sustainable utilization and expansion of ethnic medicinal resources, while laying an important foundation for the further development of

GGG stems (e.g., bioactive component isolation and pharmaceutical formulation development).

5. Conclusion

For the first time, this study integrated UPLC-Q-TOF-MS, GNPS molecular networking analysis, ultraviolet (UV) spectrophotometry, and in vivo pharmacodynamic experiments to systematically investigate the chemical compositions and anti-diarrheal activities of GGG roots, stems, and fruits. The results showed that the chemical constituents of stems and roots were highly similar. A total of 28 common compounds were identified, and the triterpenoids were completely overlapped. There was no significant difference in total triterpenoid content. In contrast, GGG fruits are predominantly composed of phenolic acids and flavonoids, showing significant chemical differences from roots and stems. In terms of efficacy, the inhibitory effect of SOE on castor oil-induced intestinal hypermotility in mice was comparable to that of ROE, while both were more effective than FOE. Joint analysis revealed that the five shared core bioactive components—including epicatechin and 16α-hydroxygypsogenic acid—possess distinct anti-inflammatory and anti-diarrheal mechanisms. Notably, the key bioactive components of fruits differ significantly from those of roots and stems. This study thus provides sufficient experimental evidence to support the use of GGG stems as an alternative medicinal part to roots. Future research can focus on the clinical translation of GGG stem-based medicinal resources, with the aim of achieving the comprehensive utilization of GGG roots, stems, and fruits.

Credit Author Statement

Jingmei Chen: Writing-original draft, Methodology, Data curation, Conceptualization. **Yuhang Chen:** Writing-original draft, Data curation, Conceptualization. **Xiaole Zhao:** Writing-original draft, Methodology, Conceptualization. **Zhilin Bai:** Methodology, Data curation. **Wenqian Wang:** Visualization, Investigation. **Lianfan Wang:** Visualization, Investigation. **Jingze Zhang:** Writing-review & editing, Supervision. **Dailin Liu:** Writing-review & editing, Supervision.

Conflict of Interest Statement

The authors declare that they have no known competing financial interests or personal relationships that could have appeared to influence the work reported in this paper.

Data Availability

Data will be made available on request.

Acknowledgments

This research did not receive any specific grant from funding agencies in the public, commercial, or not-for-profit sectors.

References

[1] Zhen, Y., Yansheng, W., Xinrui, W., Xiqin, D., Guotong, L., Lifei, L., Bin, Y., Jingze, Z., Feng, Z., & Dailin, L. (2024). The fruit of Rosa odorata sweet var. gigantea (Coll. et Hemsl.) Rehd. et Wils attenuates chronic atrophic gastritis induced by MNNG and its potential mechanism. J Ethnopharmacol. https://doi.org/ 10. 1016/ j. jep. 2024.118876.

[2] Yang, J. (2014). Chemical Constituents from Rose odorata Sweet var. gigantea andSwertia angustifolia Buch.var. pulchella. *Science of Chinese Traditional Medicine*.

[3] Lv, K., Li, J., Wang, C., He, L., Quan, S., Zhang, J., & Liu, D. (2021). Triterpenoids from Rosa odorata Sweet var. gigantea (Coll.et Hemsl.) Rehd.et Wils and their chemotaxonomic significance. *Biochemical Systematics and Ecology*. https://doi. org/10.1016/j.bse.2021.104240.

[4] AN Ying, ZHAO Yan-min, ZHANG Yue, & Dai-lin, L. (2014). Determination of total tannin in different parts ofRose odorata Sweet var. gigantean (Coll.et Hemsl.) Rehd.et Wils %J Journal of Logistics University of PAPF. *Medical Sciences*, *23*(09), 721–724.

[5] Li, X., Liu, R., Zhao, Y., Gao, N., Jin, X., Gao, X., Li, T., & Liu, D. (2020). The extract from the roots of Rose odorata sweet var. gigantean (Coll. et Hemsl.) Rehd. et Wils attenuates DSS-induced ulcerative colitis by regulating the Nrf2/NF-κB signaling pathways. *RSC Adv*, *10*(16), 9450–9461. https://doi. org/10.1039/c9ra10747a.

[6] Shuai, Q. (2020). Research on the Antidiarrheal Components of the Fruit ofRose odorata Sweet var. gigantea. *Journal of* Tianjin University of Traditional Chinese Medicine. https://doi. org/ 10.27368/d.cnki.gtzyy.2020.000562.

[7] Prevention, D. o. V., Feed Hygiene, F. o. V. M., University of Warmia, Mazury in Olsztyn, O., 10-718 Olsztyn, Poland, Feed Hygiene, F. o. V. M., University of Warmia, & Mazury in Olsztyn, O., 10-718 Olsztyn, Poland. (2017). The influence of a natural triterpene preparation on the gastrointestinal tract of gilts with streptozocin-induced diabetes and on cell metabolic activity *Journal of Functional Foods*, *33*, 11–20. https:// doi. org/ 10.1016/j.jff.2017.03.019.

[8] Yongyi, L., Zhirong, C., Ying, L., Juanjuan, G., Rong, T., Jixin, L., Yi, L., & Jun, L. (2021). Integrated molecular networking strategy enhance the accuracy and visualization of components identification: A case study of Ginkgo biloba leaf extract. *Journal of pharmaceutical and biomedical analysis*. https:// doi.org/ 10.1016/j.jpba.2021.114523.

[9] Junqi, B., Qiyu, Z., He, S., Baosheng, L., Ping, W., Juan, H., Danchun, Z., Lu, G., Wen, X., Jing, Z., Zhihai, H., & Xiaohui, Q. (2024). Processing of Reynoutria multiflora: transformation of catechin and gallic acid derivatives and their identification. *Frontiers in pharmacology*. https://doi. org/10.3389/ fphar. 2024. 1356876.

[10] Gong, J., Li, L., Lin, Y. X., Xiao, D., Liu, W., Zou, B. R., Tian, X., Han, B., Zhang, S. B., Lin, L., Li, P., Xie, Z. Y., & Liao, Q. F. (2020). Simultaneous determination of gallic acid, methyl gallate, and 1,3,6-tri-O-galloyl-β-d-glucose from Turkish galls in rat plasma using liquid chromatography-tandem mass spectrometry and its application to pharmacokinetics study. *Biomed Chromatogr*, *34*(10), e4916. https://doi. org/10. 1002/ bmc.4916.

[11] Marek, B., Peter, L., Florian, C. S., & Dietmar, R. K. (2020). Characterization of Secondary Metabolites in Flowers of Sanguisorba officinalis L. by HPLC-DAD-MS n and GC/MS. *Chemistry & biodiversity*. https://doi.org/10. 1002/cbdv. 2019 00724.

[12] Mei-Chih, L., Jih-Hui, L., Chen, S. K., Yufang, C., & Hui, C. (2020). Simultaneous determination of podophyllotoxin, quercetin and kaempferol in podophyllin by liquid chromatography tandem mass spectrometry. *Journal of Food and Drug Analysis*. https://doi.org/10.38212/2224-6614.2320.

[13] Ágnes, M. M., Virág, L., Gertrud, E. M., & Péter, G. O. (2020). High-performance thin-layer chromatography hyphenated to high-performance liquid chromatography-diode array detection-mass spectrometry for characterization of coeluting isomers. *Talanta*. https://doi.org/ 10.1016/j. talanta. 2020. 1213 06.

[14] Lihua, Z., Yan, X., Ya, X. U., Lulu, Z., Wenwen, D., Mengning, L., Hui, L., & Zhixin, W. (2024). Comprehensive characterization of anthraquinones in Damnacanthus indicus using mass spectrometry molecular networking and metabolomics-based herb discrimination. RSC Advances. https: // doi.org/10.1039/d4ra06732k.

[15] Allegra, T. A., Emily, C. G., Kerry, L. M., Louis-Félix, N., Mélissa, N.-E., Amina, B., Daniel, P., Julia, M. G., Nicole, S., Fernando, V., Justin, J. J. v. d. H., Madeleine, E., Kyo Bin, K., Christine, M. A., Andrés Mauricio, C. R., Irina, K., Kelly, C. W., Samuel, B., Catherine, R.,…Pieter, C. D. (2019). Reproducible Molecular Networking of Untargeted Mass Spectrometry Data Using GNPS. *Analytical chemistry*. https: // doi. org/10.26434/chemrxiv. 9333212. v1.

[16] Florent, O., Fanny, R., Marc, L., & David, T. (2017). Optimized experimental workflow for tandem mass spectrometry molecular networking in metabolomics. *Analytical and bioanalytical chemistry*. https://doi.org/10.1007/s00216-017-0523-3.

[17] Jun Sang, Y., Louis-Félix, N., Mingxun, W., Dong-Hyun, K., Pieter, C. D., Kyo Bin, K., & Hye Hyun, Y. (2022). Tandem Mass Spectrometry Molecular Networking as a Powerful and Efficient Tool for Drug Metabolism Studies. *Analytical chemistry*. https://doi.org/10.1021/acs.analchem.1c04925.

[18] Kaylan, R., Maria, A. S., Stafford, G. I., & Nokwanda, P. M. (2022). Mass Spectrometry Metabolomics and Feature-Based Molecular Networking Reveals Population-Specific Chemistry in Some Species of the Sceletium Genus. *Frontiers in nutrition*. https://doi.org/10.3389/fnut.2022.819753.

[19] Weibo, Q., Yi, W., Wenyi, G., & Yang, W. (2024). Application of molecular networking to improve the compound annotation in liquid chromatography-mass spectrometry-based metabolomics analysis: A case study of Bupleuri radix. *Phytochemical analysis: PCA*. https://doi.org/10.1002/ pca. 34 12.

[20] Mariana de Souza, M., Bárbara Sayuri, B., Lucas Campos Curcino, V., & Olívia Moreira, S. (2021). Use of Molecular Networking for Compound Annotation in Metabolomics. *Revista Virtual de Quimica*. https://doi.org/10.21577/1984-6835.20210116.

[21] Yoshiyasu, T. (2024). Reevaluating statistical methods in metabolomic studies: A case for Spearman's correlation. *Molecular plant*. https://doi.org/10.1016/j.molp.2024.12.014.

[22] Spearman's rank correlation coefficient. (2018). BMJ (Clinical research ed.). https://doi.org/10.1136/bmj.k4131.

[23] Qingyang, Z. (2023). On relationships between Chatterjee's and Spearman's correlation coefficients. *arXiv (Cornell University)*. https: //doi.org/10.48550/arxiv.2302.10131.

[24] Spearman Rank Order Correlation. (2022). The SAGE Encyclopedia of Research Design. https://doi.org/10.4135/ 9781071812082.n583.

[25] Teng, W., Jialong, L., Qiaqia, H., Yanmin, Z., Xiaoxia, G., Jingze, Z., & Dailin, L. (2023). Fruit of Rosa odorata Sweet var. gigantea (Coll. et Hemsl.) Rehd. et Wils Attenuates DSS-induced Ulcerative Colitis by Adjusting Nrf2/NF-κB Signaling Pathway. *Pharmacognosy Magazine*. https://doi.org/ 10.1177/ 09731296231170095.

[26] Münir, Ö., Kandikre Ramaiah, S., Maryam, S., Volkan, A., & Francisco Martín, H. M. (2023). Ethnic Knowledge and Perspectives of Medicinal Plants. https://doi. org/10. 1201/ 9781003353089.

[27] Junfeng, T., Jean-Paul, V., Annemiek van, Z., Roelant, H., Lin, Z., & Wouter, J. C. d. B. (2023). Presence of free gallic acid and gallate moieties reduces auto-oxidative browning of epicatechin (EC) and epicatechin gallate (ECg). *Food chemistry*. https://doi.org/10.1016/j.foodchem.2023.136446.

[28] Zahra, M., Eleonora, C., Jiye, K., & Patricia, I. O. (2023). Effects of (-)-epicatechin on hepatic triglyceride metabolism. *Food & function*. https://doi.org/10.1039/d3fo03666a.

[29] Huimin, Y., Huixia, H., Zhihao, W., Dawei, Y., Juan, K., & Jun, L. (2022). Structure, stability and antioxidant activity of dialdehyde starch grafted with epicatechin, epicatechin gallate, epigallocatechin and epigallocatechin gallate. *Journal of the science of food and agriculture*. https://doi.org/10. 1002/ jsfa. 12003.

[30] Thomas, S., Andrzej, M., Marc, B., Dragan, M., Anne-Françoise, S., Christine, M., & Aurélien, L. (2015). Epicatechin Impact on Primary Hemostasis, Coagulation and Fibrinolysis [Article INRA, Clermont-Ferrand, France CHU Clermont-Ferrand, Haematology department, Clermont-Ferrand, France INRA, Clermont-Ferrand, France CHU Clermont-Ferrand, Haematology department, Clermont-Ferrand, France INRA, Clermont-Ferrand, France CHU Clermont-Ferrand, Haematology department, Clermont-Ferrand, France]. *Blood*. https:// doi.org/10.1182/blood. v126.23.4677.4677.

[31] Xiaofei, S., Qing-Jie, K., Kaiqiang, S., Le, H., Ximing, X., Jingchuan, S., & Jiangang, S. (2020). Expression of Nogo-A in dorsal root ganglion in rats with cauda equina injury. *Biochemical and biophysical research communications*. https:// doi.org/10.1016/j.bbrc.2020.04.094.

[32] Hu, L. D., Yu, B. P., & Yang, B. (2012). Deoxycholic acid inhibits smooth muscle contraction via protein kinase C-dependent modulation of L-type Ca2+ channels in rat proximal colon. *Mol Med Rep*, *6*(4), 833–837. https://doi.org/10. 3892/ mmr. 2012.984.

[33] Xiuxiu, J., Li, L., Qinlu, P., Chunmei, G., Li, G., Siyu, H., Shuangyan, T., Wenchen, P., Yu, L., Yanqiu, G., Yuqin, Y., Gang, W., Xiaohui, L., Meng, G., Lei, P., Huiyuan, Z., Shiqian, Q., Heng, X., Hongbo, H.,…Lunzhi, D. (2022). Glycyrrhetinic acid restricts mitochondrial energy metabolism by targeting SHMT2 [Article]. *iScience*. https://doi.org/ 10.1016/j. isci. 2022. 104349.

[34] Fei, X., Zhongdaixi, Z., Lingyu, X., Chuhong, S., Junbin, C., Xiangfu, G., Jiaqi, T., Shihua, Z., Huiyu, L., & Longying, Z. (2021). Soyasaponin A 2 Alleviates Steatohepatitis Possibly through Regulating Bile Acids and Gut Microbiota in the Methionine and Choline-Deficient (MCD) Diet-induced Nonalcoholic Steatohepatitis (NASH) Mice. *Molecular nutrition & food research*. https://doi. org/10. 1002/ mnfr. 2021 00067.